Structural aspects of the relaxation process in spin crossover solids: Phase separation, mapping of lattice strain, and domain wall structure

W. Nicolazzi[1,2] and S. Pillet[1,*]

[1]*Laboratoire de Cristallographie, Résonance Magnétique et Modélisations, UMR CNRS 7036, Institut Jean Barriol, Université de Lorraine, B.P. 70239, F-54506 Vandoeuvre-lès-Nancy, France*

[2]*Laboratoire de Chimie de Coordination, CNRS UPR-8241 and Université de Toulouse, UPS, INP, F-31077 Toulouse, France*

(Received 17 June 2011; published 2 March 2012)

We present a nonequilibrium study of the relaxation process in spin crossover solids using numerical simulations of a recently introduced two-variable elastic Ising-like model. We analyze the structural lattice distortions accompanying the relaxation from the metastable high-spin to the ground low-spin state as a function of cooperativity. In the highly cooperative case, a sigmoidal relaxation behavior of the high-spin fraction n_{HS} is described, and it occurs jointly with a structural phase separation process. The mean lattice spacing follows a similar sigmoidal trend, owing to the interplay between electronic and lattice variables in the Hamiltonian. Weakly cooperative systems are characterized by single exponential relaxations of the high-spin fraction, the corresponding structural transformation proceeds homogeneously with a progressive relaxation of the mean lattice spacing. Long relaxation tail effects are also observed. We highlight the development of lattice strain accompanying the spin transition, and show that structural phase rebuilding proceeds in the late stage of the relaxation by releasing residual strain. Under specific conditions, a temporal decoupling between the electronic and lattice variables is observed, which may have direct applications for interpreting time-resolved spectroscopic or diffraction experiments and for elucidating unusual structural behaviors, such as the development of superstructures, modulated structures, or transient phases.

DOI: 10.1103/PhysRevB.85.094101 PACS number(s): 05.50.+q, 64.60.De, 75.30.Wx, 75.60.−d

I. INTRODUCTION

Functional molecular materials have been the subject of intense research activities for the last decades and are currently considered as a relevant alternative in the next generation of electronic nanodevices.[1] In this context, spin crossover (SCO) materials have attracted much attention,[2] owing to their bistability and switching properties. SCO complexes exhibit a reversible switching between molecular low-spin (LS) and high-spin (HS) states, which may be triggered by a change of temperature, pressure,[3,4] and magnetic field[5,6] or using a pulsed[7,8] or continuous optical excitation.[9,10] The bistability property is closely related to strong interactions between the molecules, the so-called cooperativity, which originates from the large HS to LS molecular volume contraction inducing local lattice distortions, coupled to long-range interactions of elastic origin within the solid;[11,12] these are mediated by intermolecular contacts between the SCO molecules.[13]

In SCO solids, a metastable HS state may be populated at very low temperature by photoexcitation from the ground LS state through the LIESST effect (light induced excited spin state trapping).[9,10] Detailed information on the out-of-equilibrium behavior, light-induced excitation, and subsequent isothermal relaxations, have been obtained using photomagnetic and optical reflectivity measurements. It has been shown that strong cooperativity in the crystal results in characteristic sigmoidal relaxation curves of the HS fraction n_{HS}. These results have been well interpreted in the framework of the macroscopic phenomenological equation of Hauser,[14,15] which considers in a mean-field approach that relaxation is a thermally activated unimolecular process whose rate is modulated by the immediate environment. A slowing down at the end of the relaxation process, the so-called "tail effect," has been further detected in some cases,[16] and attributed to the onset of strong short-range correlations[11] or to inhomogeneities, mainly due to chemical impurities and structural defects, resulting in a spatial distribution of activation energies.[17,18]

Various Ising-like models, based on a two-level fictitious spin formalism with short-range interactions, have been introduced to describe SCO phenomena;[19,20] these models have been investigated by numerical simulations,[11] exact analytical treatment of the partition function,[21] or analytical approaches using mean-field approximation.[22,23] These models capture the essential features of spin transitions, and have been further extended to interpret dynamic aspects in the relaxation,[23,24] and the photoexcitation[25] regimes. The dynamic Ising-like model in the mean-field approximation[23,25] gives a microscopic origin of the macroscopic equation of Hauser. This approach has allowed to develop analytical schemes beyond mean-field approximations, by using local equilibrium method[24] or by taking into account short-range correlations,[26] thus reproducing the "tail effect."

It is now well accepted that the formation and dynamics of like-spin domains (LSD), i.e., the clustering of adjacent molecules in the same spin state,[27] play a major role in the various spin transition phenomena. Phase separation behaviors have been evidenced by reciprocal space mapping using x-ray and neutron diffraction experiments for the most cooperative SCO systems in the thermal spin transition,[28] photoexcitation,[29] or light-induced bistability[30] regimes. The corresponding kinetics of phase separation has been further interpreted using the Kolmogorov-Johnson-Mehl-Avrami model of phase transformation from kinetic x-ray diffraction measurements.[29,31] In some cases, the subtle interplay between spin and structural degrees of freedom may lead to intriguing and unusual structural features, such as symmetry breaking transitions resulting in the development of superstructures[32–34]

or incommensurate modulated structural phases,[35] observed under specific experimental conditions of temperature, light irradiation, or under thermal quenching. More recently, LSD have been directly imaged by optical microscopy[36–38] and Raman spectroscopic techniques,[39] highlighting new aspects of the spatiotemporal development of the nucleation, domain growth and propagation of the thermodynamically stable phase. A temporal decoupling of spin and crystallographic phase transitions may also occur, as has been reported at the thermal spin transition or during the relaxation process of SCO materials.[40,41] Quite recently, detailed information has been derived on the successive temporal steps of photoinduced spin state switching by a combination of time-resolved spectroscopic and x-ray diffraction[42,43] or x-ray absorption techniques.[44] It has been shown that the electronic and structural switching span several temporal orders of magnitude from sub-picosecond (electronic processes) to nanosecond (volume expansion) and microsecond (thermal switching) time scales.

As a consequence, the spin transition phenomenon is intrinsically a multiscale process that requires an understanding of atomic scale lattice distortions as well as mesoscopic structural organizations to interpret these unusual structural behaviors, and LSD formation and dynamics. Obviously, these effects can not be interpreted within mean field and require appropriate models accounting for crystallographic aspects. In this direction, several microscopic elastic schemes that introduce explicitly lattice degrees of freedom have been recently proposed to provide a clear microscopic origin of cooperativity.[45–53] Some of these models are based on the atom-phonon treatment initially introduced by Nasser.[50] The first-order character of the spin transition is controlled by the strength of elastic constants, which can be dependent on the spin state.[45,47,48,50] Analytical solutions for a one-dimensional chain have shown that the atom-phonon model is isomorph to an Ising-like model under an effective temperature-dependent ligand field.[45,50] At higher dimension, lattice deformations lead to elastic long-range interactions, suggesting a different nucleation and domain growth process than the original Ising-like model. Monte Carlo (MC) or molecular dynamics simulations on square[47,53] and hexagonal lattices[54] using mechanoelastic models have displayed a spin conversion that nucleates preferentially from the corner and then domains propagate inside the bulk when open boundary conditions are applied to the lattice. On the contrary, purely elastic schemes with periodic boundary conditions do not display clustering process.[46] We have introduced a microscopic elastic Ising-like model (called hereafter anharmonic model), which considers a spin- and distance-dependant intermolecular coupling, aiming at providing an efficient description of the structural aspects related to the spin transition.[47] Using this scheme, photoinduced crystallographic phase separation phenomena are well reproduced[55] and the corresponding domain growth kinetics follow the Kolmogorov-Johnson-Mehl-Avrami model in agreement with the experimental x-ray diffraction findings.[29,31] Nonlinear effects of the photoexcitation, such as sigmoidal photoconversion kinetics, and the presence of an incubation time, are also retrieved.

The aim of the present study is to grasp the essential structural aspects at the microscopic and mesoscopic scales of nonequilibrium relaxation processes in SCO solids to attain a clear picture of the spatiotemporal properties using MC simulations of the anharmonic model. The paper is organized as follows. Section II is devoted to the introduction of the dynamic anharmonic model and the computational details of the MC methods. The transformation mechanisms are discussed in Sec. III, considering the evolution of the thermal relaxation curves for the spin and lattice variables, the corresponding spatial correlation functions as well as the development and mapping of local lattice strain, and microstructural characterization of domain walls.

II. KINETIC ANHARMONIC ISING-LIKE MODEL AND COMPUTATIONAL DETAILS

A. Anharmonic Ising-like model

In a previous work,[47] we have introduced an anharmonic elastic Ising-like model to describe the equilibrium properties of SCO solids. The corresponding Hamiltonian, adapted from the standard two-level Ising-like model,[19,20] writes

$$\mathcal{H}(\{\sigma\},\{\vec{r}\}) = \frac{\Delta_{\text{eff}}}{2}\sum_i \sigma_i + \sum_{\langle i,j\rangle} V_{\text{elast}}\left(r_{\langle i,j\rangle}, r^0_{\langle i,j\rangle}\right) \times [J_0 + J_1(\sigma_i + \sigma_j) + J_2\sigma_i\sigma_j]. \quad (1)$$

The two degenerated molecular states are represented by fictitious Ising spin operators $\hat{\sigma}$, whose eigenvalues $\sigma = +1$ and $\sigma = -1$ are assigned to the HS and the LS states, respectively, with g_+ and g_- the corresponding vibronic degeneracies ($g_+ \gg g_-$). The first term on the right-hand side in Eq. (1) corresponds to the on-site Hamiltonian for a system of N SCO entities, where $\Delta_{\text{eff}} = \Delta - k_B T \ln(g_+/g_-)$ and Δ is the energy difference between the HS and LS ground states. To capture the essential intermolecular interactions in SCO molecular solids, the interaction energy [second term in Eq. (1)] is developped on pairwise 6-3 Lennard-Jones (LJ) potentials with finite-range $r_{\max}$ as given in Eq. (2):

$$\begin{aligned} &\text{if} \quad r_{\langle i,j\rangle} \leqslant r_{\max}, \\ &\quad V_{\text{elast}}\left(r_{\langle i,j\rangle}, r^0_{\langle i,j\rangle}\right) = \left(\frac{r^0_{\langle i,j\rangle}}{r_{\langle i,j\rangle}}\right)^6 - 2\left(\frac{r^0_{\langle i,j\rangle}}{r_{\langle i,j\rangle}}\right)^3, \\ &\text{if} \quad r_{\langle i,j\rangle} > r_{\max}, \\ &\quad V_{\text{elast}}\left(r_{\langle i,j\rangle}, r^0_{\langle i,j\rangle}\right) = 0. \end{aligned} \quad (2)$$

$r_{\langle i,j\rangle} = |\vec{r}_i - \vec{r}_j|$ and $r^0_{\langle i,j\rangle} = |\vec{r}^{\,0}_i - \vec{r}^{\,0}_j|$ are the neighboring instantaneous and equilibrium distances, respectively, between site i and j. They correspond to the Fe. . . Fe distances in SCO molecular crystals and are assimilated to lattice spacings hereafter. In the following, we set $r_{\max}$ to 1.5. To account for the different structural (e.g., lattice spacing) and elastic (e.g., Bulk modulus, thermal expansion) properties between purely HS and LS phases, three distinct V_{elast} potentials are considered, with equilibrium distances r^0_{HS}, r^0_{LS}, and r^0_{HL} for HS-HS, LS-LS, and HS-LS neighboring pairs. In this scheme, the interaction energy depends on the respective spin state and separation distance between neighboring molecules. We consider that this is of paramount importance to account for

local structural relaxations and lattice distortions accompanying the spin state switching and therefore to describe structural phase transition and phase separation phenomena. Within this elastic scheme, the spin and lattice variables are coupled directly in the Hamiltonian. The spin-state switching of one molecule generates a local lattice distortion owing to the spin dependence of the V_{elast} potential, which in turn affects the whole lattice through the intermolecular interactions. Effective long-range interactions result from this scheme, even though only short-range interactions are formally present in the Hamiltonian. This is at variance with the classical short-range Ising-like model applied to SCO solids.

The parameters of the anharmonic model can fluctuate with temperature when the system is in contact with a thermal bath. We define two observables whose thermal averages are the usual HS fraction n_{HS}:

$$n_{\text{HS}} = \frac{1 + \langle \sigma \rangle}{2}, \tag{3}$$

directly related to the mean "magnetization" $\langle \sigma \rangle$, and a dimensionless and normalized lattice spacing r^{norm},

$$r^{\text{norm}} = \frac{\langle r \rangle - r^0_{\text{LS}}}{r^0_{\text{HS}} - r^0_{\text{LS}}}, \tag{4}$$

where $\langle r \rangle = \langle r_{\langle i,j \rangle} \rangle$ is the mean intersite distance. As already introduced for the standard Ising-like model, first-neighbor spin spatial correlations are given by

$$C_{\sigma,\sigma'}(t) = \frac{1}{N} \sum_{\langle i,j \rangle} \langle \sigma_i \sigma_j \rangle. \tag{5}$$

The HS-LS nearest-neighbor pair fraction, noted n_{HL}, is related to the spin spatial correlation function $C_{\sigma,\sigma'}(t)$ through the relation[24]

$$n_{\text{HL}}(t) = \frac{1 - C_{\sigma,\sigma'}(t)}{4}. \tag{6}$$

In a similar way, we define a spatial correlation function written as

$$C_{r,r'}(t) = \frac{\sum_{\langle k,l \rangle} \langle r_k r_l \rangle - M \times \langle r \rangle^2}{M \times \langle r \rangle^2}, \tag{7}$$

where $\langle k,l \rangle$ corresponds to nearest-neighbor intersite bonds. M is the realizable number of product between nearest-neighbor bonds with the free boundary conditions; it normalizes the correlation function. $C_{r,r'}$ probes the extent of spatial structural distortion; a zero value of $C_{r,r'}$ corresponds to a nondistorted lattice with a uniform thermal mean intersite distance $\langle r \rangle$.

The numerical study of the static and quasistatic thermodynamic properties[47] has revealed that the anharmonic model exhibits an order-disorder thermal transition at a critical temperature T_C, different from the second-order critical temperature of the Ising model under zero field, due to the existence of both short-range Ising coupling and effective long-range interactions, mediated by elastic couplings.[56] The anharmonic model can reproduce gradual or abrupt thermal transitions, with or without thermal hysteresis, by fine tuning the values of the model parameters, especially J_2 (see Fig. 1). It is noteworthy that the $J_2 = 0.5$ case exhibits a gradual two-step transition, resulting from the competition between short-range and long-range interactions; an ordered pattern of HS and LS species is, however, not formed under such conditions.

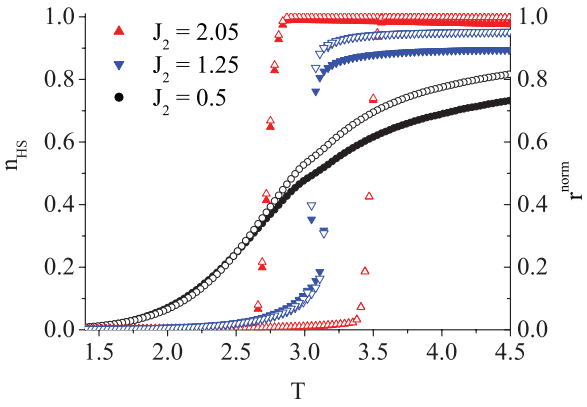

FIG. 1. (Color online) HS fraction n_{HS} (open symbols) and normalized lattice spacing r^{norm} (filled symbols) as a function of temperature, for different values of the J_2 coupling parameter. Thermal cycles have been computed as in Ref. 47, using the Metropolis MC dynamic for the two variables, thermal averages have been computed over 5000 independent MC simulations. Model parameters are $J_0 = 1000$, $J_1 = 0.15$, $\Delta = 7.2$, and $\ln g = 2$.

B. Kinetic anharmonic model

For investigating the relaxation process, we consider a MC method as follows. Let $\mathcal{P}(\{\sigma\},\{\vec{r}\})$ be the probability for the system to adopt the spin and lattice configuration $(\{\sigma\},\{\vec{r}\})$ at time t. We assume that the temporal evolution of $\mathcal{P}(\{\sigma\},\{\vec{r}\})$ is governed by the two-variable microscopic master equation:

$$\frac{\partial \mathcal{P}(\{\sigma\},\{\vec{r}\},t)}{\partial t} = \int \prod_{i=1}^{N} d\vec{r}_i' \sum_{\{\sigma'\}} (\Omega(\{\sigma'\},\{\vec{r}'\} \to \{\sigma\},\{\vec{r}\}) \times \mathcal{P}(\{\sigma'\},\{\vec{r}'\},t) - \Omega(\{\sigma\},\{\vec{r}\} \to \{\sigma'\},\{\vec{r}'\}) \times \mathcal{P}(\{\sigma\},\{\vec{r}\},t)), \tag{8}$$

where $\Omega(\{\sigma'\},\{\vec{r}'\} \to \{\sigma\},\{\vec{r}\})$ is the transition rate. The choice of the transition rate Ω is fundamental when nonequilibrium kinetics is considered. Its rigorous establishment should be based on the knowledge of microscopic processes, resulting from quantum-mechanical considerations. It has to retrieve the Boltzmann equilibrium distribution in the stationary state $\partial \mathcal{P}(\{\sigma\},\{\vec{r}\})/\partial t = 0$, and the detailed balance condition is imposed:

$$\frac{\Omega(\{\sigma'\},\{\vec{r}'\} \to \{\sigma\},\{\vec{r}\})}{\Omega(\{\sigma\},\{\vec{r}\} \to \{\sigma'\},\{\vec{r}'\})} = \frac{\exp[-\beta \mathcal{H}(\{\sigma\},\{\vec{r}\})]}{\exp[-\beta \mathcal{H}(\{\sigma'\},\{\vec{r}'\})]}. \tag{9}$$

In SCO compounds, the suitable dynamics would account for the transition probability from a HS vibrational state to a LS one for a single molecule in contact with a thermal bath and an intermolecular phonon bath, corresponding to lattice vibrations.[57] In the following, we decouple the total transition rate Ω in separate spin and lattice contributions, noted $W_{\text{spin}}(\{\sigma'\} \to \{\sigma\})$ and $W_{\text{elast}}(\{\vec{r}'\} \to \{\vec{r}\})$. Spin and lattice degrees of freedom interact individually with the heat bath, inducing stochastically their reversal and incremental

modification, respectively. This particular choice is justified by the different characteristic time scales at which electronic processes (femtosecond) and nuclear displacements (picosecond to nanosecond) occur. It is well known that for SCO materials, the photoexcitation and thermal relaxation outside the tunnel regime are thermally activated processes,[15] related to the crossing of energy barriers in a purely classical point of view. Accordingly, as suggested for the standard dynamic Ising-like model, a transition rate of Arrhenius type is well suited,[23,58] for which a microscopic origin has recently been provided by expressing the "exchange" interactions in the Ising-like model as spin-phonon couplings.[59] There exists several forms of Arrhenius dynamics.[60] We adopt here, a "one-step dynamic" (OSD),[61] noted hereafter W_{OSD}, which corresponds to the transition probability from an initial state of energy E_i to a final state of energy E_f, passing through an intermediate state ("saddle point") of energy E_T. W_{OSD} can be written in the general form

$$W_{\mathrm{OSD}} \sim \exp[-\beta(E_T - E_i)]. \tag{10}$$

The expression for E_T is simply

$$E_T = \frac{E_i + E_f}{2} + E_{\mathrm{barrier}}, \tag{11}$$

where E_{barrier} corresponds to a microscopic energy barrier. In the next, we use the same writing proposed in other previous work[23] for the spin dynamic,

$$W_{\mathrm{spin}}(\{\sigma\} \to \{\sigma'\}) = \frac{1}{\tau^0_{\mathrm{spin}}} e^{-\beta[E_{\mathrm{spin}} - \frac{E_i}{2}]}, \tag{12}$$

and for the lattice dynamic,

$$W_{\mathrm{elast}}(\{\vec{r}\} \to \{\vec{r}'\}) = \frac{1}{\tau^0_{\mathrm{elast}}} e^{-\beta[E_{\mathrm{elast}} - \frac{E_i}{2}]}. \tag{13}$$

$1/\tau^0_{\mathrm{spin}}$ and $1/\tau^0_{\mathrm{elast}}$ correspond to an intrinsic intramolecular frequency associated to spin and lattice state switchings, respectively. In contrast with previous results,[23,58] E_{spin} and E_{elast} are assimilated to nonconstant intramolecular and intermolecular energy barriers, which are sensitive to the local environment since they are function of the energy of the final state:

$$\begin{aligned} E_{\mathrm{spin}}(\{\sigma'\},\{\vec{r}\}) &= E^0_{\mathrm{spin}} + \frac{E_f(\{\sigma'\},\{\vec{r}\})}{2}, \\ E_{\mathrm{elast}}(\{\sigma\},\{\vec{r}'\}) &= E^0_{\mathrm{elast}} + \frac{E_f(\{\sigma\},\{\vec{r}'\})}{2}, \end{aligned} \tag{14}$$

where E^0_{spin} and E^0_{elast} are phenomenological parameters corresponding to a reference for intra and intermolecular energy barriers.

C. Computational details

The dynamic properties of the Hamiltonian (1) are studied using MC methods. It is important to distinguish the variable t in the MC approach, which defines the time unit called Monte Carlo step (MCS), from the real time from Newtonian classical equations or the Schrodinger equation in quantum mechanics. The MC time is defined arbitrarily and depends on the different processes included in a MCS, giving a certain disadvantage compared to other algorithms, integrating directly the dynamical equations, as, for example, molecular dynamics.[48,52] Especially, the direct comparison with experimental kinetic data is impossible. MC methods are nevertheless advantageous to calculate thermodynamic quantities. In the next, we consider a system of 32×32 ($N = 1024$) spins on a deformable two-dimensional lattice with the free boundary conditions, allowing energy, and "volume" fluctuations. The model parameters are set to $J_0 = 1000$, $J_1 = 0.15$, $\Delta = 7.2$, and $\ln g = 2$. Equilibrium lattice spacings of HS, LS, and intermediate HS-LS structural phases are set to $r^0_{\mathrm{HS}} = 1.2$, $r^0_{\mathrm{LS}} = 1$, and $r^0_{\mathrm{HL}} = 1.1$, respectively.

Thermal relaxations after a quench are investigated through the n_{HS} and r^{norm} temporal evolutions, calculated numerically by ensemble averages; temporal averages are not valid owing to the absence of ergodicity and to the breaking of translation invariance in time. Practically, thermal means are performed on a set of 20 000 identical independent configurations of systems. A MCS corresponds to the three following stages: (i) a site i and a normalized number p are chosen randomly; the fictitious spin σ_i flip is updated according to the Arrhenius dynamic for the spin variable W_{spin}. If $p < W_{\mathrm{spin}}$, the new spin configuration is accepted. (ii) A second site j at the position $\vec{r}_j\,(x_j, y_j)$ and an other normalized number p' are chosen randomly; a new position $\vec{r}'_j(x'_j, y'_j)$ is proposed as follows:

$$x'_j = x_j + d_{x_j}, \quad y'_j = y_j + d_{y_j}, \tag{15}$$

where d_{x_j} and d_{y_j} are continuous displacement drawn on a gaussian distribution with zero mean and adjustable variance. The new position is evaluated and accepted if $p' < W_{\mathrm{elast}}$. (iii) The two previous sequences are repeated N times. The transition probabilities should be normalized in the Arrhenius dynamic[58] to satisfy the two following inequalities:

$$0 < W_{\mathrm{spin}} < 1, \quad 0 < W_{\mathrm{elast}} < 1. \tag{16}$$

In the simulation, all new configuration propositions inducing a transition rate that does not satisfy these two inequalities, will be systematically rejected. In all calculations, we set $E^0_{\mathrm{spin}} = 10$ and $E^0_{\mathrm{elast}} = 5$, and $\tau^0_{\mathrm{spin}} = 0.8$, and $\tau^0_{\mathrm{lattice}} = 1.0$.

D. Local strain mapping

Our simulations are performed on a deformable 2D lattice with equilibrium intersite distances r^0_{HS} (respectively, r^0_{LS}) corresponding to purely HS (respectively, LS) structural phases. Along the relaxation path, large structural deformations may occur induced by the HS-LS difference in intersite distances. Strain tensors are the primary measure of such local deformations in continuum mechanics, and may be computed from the gradient of a continuous displacement field with respect to a reference lattice. Local strain tensors may be derived in a discrete form by considering the local distortion around each lattice site with respect to a reference structural configuration.[62,63] We first consider two reference regular square lattices, namely HS and LS, in which each site is surrounded by four neighbors with r^0_{HS} and r^0_{LS} intersite

separation distance, respectively. For a given structural configuration of the lattice, a transformation matrix J_i is assigned to each site i. The local affine transformation matrix J_i, which best describes (in the least-squares sence) the deformation of the nearest-neighbor environment of site i with respect to the corresponding HS or LS reference lattice, is calculated by minimization of the quantity

$$\sum_j \left|\vec{r}_{ij}^{\,0} J_i - \vec{r}_{ij}\right|^2, \tag{17}$$

where $\vec{r}_{ij}$ is the current position vector between sites i and j and $\vec{r}_{ij}^{\,0}$ is the corresponding reference (HS or LS) position vector; the summation runs over all nearest neighbors of site i. The local Lagrangian strain matrix associated to site i is then computed as

$$\epsilon_i = \tfrac{1}{2}\left(J_i J_i^T - I\right). \tag{18}$$

In the following, to map the local strain on the simulation lattice, and therefore quantify local structural distortions, we use the invariant $\mathrm{Tr}\,(\epsilon_i)$ of the ϵ_i matrix; it corresponds to the relative volume variation of the immediate neighborhood of the considered molecule i.

III. RESULTS OF THERMAL RELAXATION AFTER A QUENCH

Thermal relaxation after a quench to low temperature is investigated as follows. The system is initially prepared in the totally HS electronic ($n_{\mathrm{HS}} = 1$) and HS structural configuration ($r^{\mathrm{norm}} = 1$). At $t = 0$, the system is quenched to low temperature ($T = 1.8$), outside the spinodal regime and at which the HS configuration becomes metastable, and is allowed to evolve under the stochastic dynamics. Various aspects of the relaxation to the LS ground state are probed through the nonequilibrium kinetics of the n_{HS} and r^{norm} variables as a function of time (in MCS); these relaxation curves are discussed in the next section.

A. n_{HS} and r^{norm} relaxation curves

The influence of the J_2 parameter on the relaxation curves is investigated. We have shown previously for the thermal transition regime[47] that J_2 drives the abruptness of the thermal transition, and therefore the first-order character, while J_0 plays only a minor role. An increase of J_2 leads to an enhancement of the coupling between spin and lattice degrees of freedom, and therefore of the SCO cooperativity.

For the standard Ising-like model, the short-range coupling parameter J drives the sigmoidal character of the relaxation of n_{HS}, as shown by kinetic analytical[22–24] or MC simulations[58] from a dynamic Ising-like model. Similarly for the present anharmonic model, for strong values of the J_2 parameter ($1.45 \leqslant J_2 \leqslant 2.15$), the relaxation curves of the HS fraction n_{HS} follow a sigmoidal trend (see Fig. 2), characteristic of the self-accelerated phenomenon. Owing to the interplay between spin and lattice variables in the Hamiltonian, the mean lattice spacing follows a similar sigmoidal trend from $r^{\mathrm{norm}} = 1.0$ to $r^{\mathrm{norm}} \to 0$. As the cooperative relaxation proceeds, molecules in the HS electronic configuration progressively switch to the LS electronic state, giving rise to local lattice distortions. As

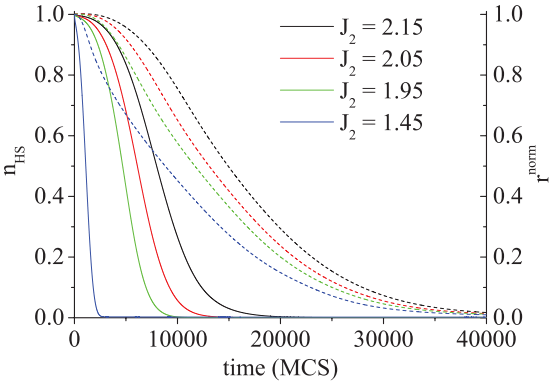

FIG. 2. (Color online) Relaxation curves for the HS fraction n_{HS} (full lines) and the normalized lattice spacing r^{norm} (dashed lines) for different "strong" values of the J_2 parameter ($1.45 \leqslant J2 \leqslant 2.15$).

a consequence, the mean lattice spacing gradually contracts from a purely HS structural phase to a purely LS phase. We note on Fig. 2 that the relaxation of the lattice spacing is systematically delayed from the n_{HS} relaxation. This results from the deliberate choice of two independent MC dynamics for the spin and lattice degrees of freedom, with different characteristic times ($\tau^0_{\mathrm{spin}} < \tau^0_{\mathrm{lattice}}$), and from the continuous character of the lattice variables. We have indeed analyzed the relaxation process with different ratios of the characteristic times (not shown here), and found that the corresponding relaxation curves may be significantly influenced. As J_2 decreases, the sigmoidal character of the n_{HS} relaxation curve attenuates, corresponding to a decrease of the cooperativity of the system; this result corroborates recent simulations of thermal relaxation with an elastic model on a hexagonal lattice.[49] The lifetime of the metastable state shortens, as clearly illustrated by the short time behaviors, the escape from the HS metastable state becomes easier with the weakening of the cooperativity, corresponding to a lowering of the energy barrier. In parallel, the delay between r^{norm} and n_{HS} tends to increase with the decrease of the J_2 parameter, indicating that the molecule-lattice coupling weakens. The well-known tail effect, corresponding to a slowing down of the relaxation of n_{HS} at long time, originating from the onset of short-range correlations[22,26] is clearly observed and tends to disappear as J_2 decreases. The magnetoelastic coupling J_2 plays therefore a major role in the short-range correlations within the lattice and drives the local structural distortions.

As the J_2 parameter further decreases ($0.5 \leqslant J_2 \leqslant 1.20$), the n_{HS} relaxation curves become progressively single exponential or stretched single exponential [see Fig. 3(a)]. On the contrary, the r^{norm} relaxation curves do not show any noticeable evolution for J_2 below 1.20 [see Fig. 3(b)]. The n_{HS} relaxation seems to be much more influenced by the decrease of cooperativity than the mean lattice spacing. In this weakly cooperative case, it is therefore expected that the elastic properties are almost independent on the spin state, and correlatively do not vary along the relaxation process. At variance, for strongly cooperative materials, the elastic properties, such as thermal expansion tensor, bulk modulus, sound velocity or Debye temperatures, may depend on the spin state. As a matter of fact, experimental evidences have

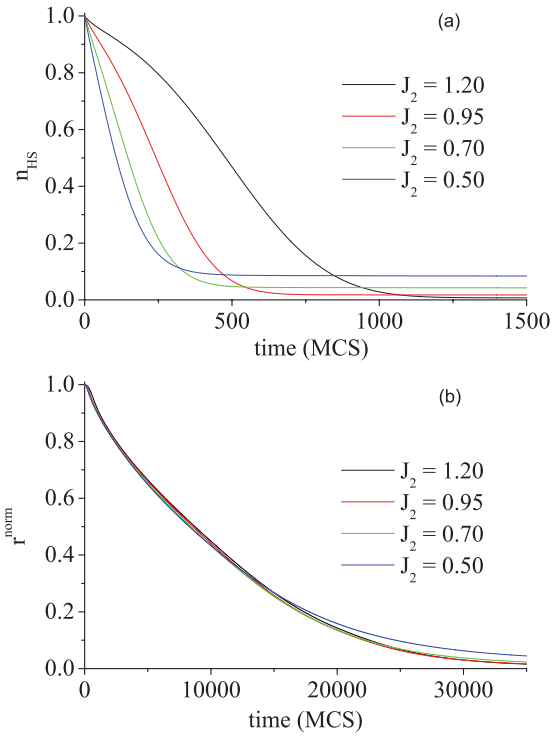

FIG. 3. (Color online) Relaxation curves for (a) the HS fraction n_{HS} and (b) the normalized lattice spacing r^{norm} for different "weak" values of the J_2 parameter.

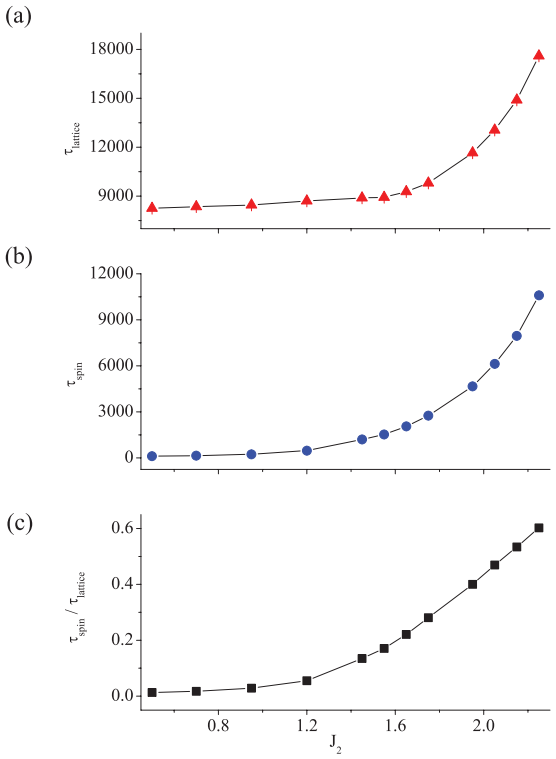

FIG. 4. (Color online) Evolution of (a) the lattice relaxation time $\tau_{lattice}$, (b) the spin relaxation time τ_{spin}, and (c) the $\tau_{spin}/\tau_{lattice}$ ratio as a function of the J_2 parameter. Relaxation times are defined as the half-life (in MCS) of the metastable HS phase ($n_{HS} = 0.5$ and $r^{norm} = 0.5$ for spin and lattice, respectively).

been provided by x-ray diffraction[64] that the thermal expansion tensors in the HS and LS phases differ for the cooperative SCO material $[Fe(btr)_2(NCS)_2] \cdot H_2O$, while spectroscopic ellipsometry measurements and diffuse reflectivity measurements under pressure[65] have shown that the bulk modulus, sound velocity, and Debye temperature may also change along the charge transfer transition in a prussian blue analog molecular solid. Within the present anharmonic model, since the V_{elast} potential is dependent on the spin states of neighboring molecules as defined in Eq. (2), it has been found that the resulting linear thermal expansion coefficients are different in the HS and LS phases.[47]

For such weak J_2 couplings, the time scale at which the thermal relaxation of n_{HS} and r^{norm} occurs is completely different: a thousand MCS is sufficient for the molecules to adopt the LS equilibrium electronic configuration whereas complete relaxation of the lattice requires more than 30 000 MCS steps. We anticipate that this behavior may found interesting applications in time-resolved experiments, which have shown that the electronic (spin state) and lattice degrees of freedom respond to photoexcitation with different time scales.[42] However, it has to be kept in mind that the arbitrary character of the "Monte Carlo time" (or Monte Carlo step) prevents a quantitative comparison with the real time of an experiment.

The interplay between spin and lattice variables is well illustrated by the mutual inspection of the relaxation time τ_{spin} and $\tau_{lattice}$ (see Fig. 4). These are defined as the half-life (in MCS) of the HS phase from the spin and lattice points of view. As J_2 increases, a clear enhancement of the relaxation time occurs, correlated to an increase of the lifetime of the HS metastable state. In parallel, spin and lattice variables becomes much more coupled [see Fig. 4(c)]. For weak J_2 values, the relaxation time ratio $\tau_{spin}/\tau_{lattice}$ is close to zero since the spins relax faster than the lattice variable by several orders of magnitude. On the contrary, for strong J_2 values, the ratio reaches almost 0.7, molecules and lattice relaxation takes place in very similar time scales.

B. Like-spin domain formation and structural phase separation

Short-range correlations and LSD formation and dynamics play a major role in the properties of cooperative spin transitions both in the quasistatic and in the out-of-equilibrium regimes, resulting, for instance, in the nonlinearity of light-induced thermally induced and relaxation dynamics, and in the presence of long relaxation tails; this is well documented from photomagnetic and optical reflectivity experiments. From the modeling point of view, the effective interaction range in elastic Ising-like models is of paramount interest.[66] Recent focus has been attached to the simulation of nanoparticle finite-size SCO systems,[67,68] for which the extent of long-range interactions with respect to the system (particle) size in addition to edge effects in open boundary conditions are of major concern. As discussed in Sec. II A, the present anharmonic model relies on a combination of short-range and effective long-range interactions, which results in the nucleation and growth of LSD in the case of highly cooperative thermal transitions, as we recently reported.[47] Experimentally, the presence of LSDs has been emphasized from x-ray and

neutron diffraction experiments, evidenced by so-called Bragg peak splitting, and imaged by optical microscopy[36–38] and Raman spectroscopic techniques.[39] However, these different types of experiment focus on very different aspects of the spin transition phenomenon. Spectroscopic techniques (optical absorption, optical reflectivity, Mössbauer) or magnetic measurements give a signal directly related to the HS fraction n_{HS}. On the contrary, diffraction experiments probe structurally ordered regions of a single crystal or polycrystalline sample. Spectroscopic or magnetic measurements do not even require the sample to be crystalline. The present two-variable anharmonic model affords the possibility of describing the SCO phenomenon using both aspects. In the following, we propose to distinguish molecular like-spin domain (MLSD) from structural like-spin domain (SLSD). MLSD defines the clustering of molecules with the same electronic configuration (HS or LS), it has a clearly defined domain boundary. The size of MLSD can be related to the spatial spin correlation function by the Fourier transform of the two-site spin correlation functions, the so-called structure function.[69] SLSD is an extended region of the system in which the structure (intramolecular, lattice spacing, and orientation) is well defined and perfectly ordered and differs from the neighboring regions. SLSD can be characterized from scattering techniques (diffraction and diffusion) and quantitative analysis of the diffraction pattern. For instance, the domain size and domain boundary thickness have been extracted from high-resolution x-ray diffraction experiments or electron microscopy for ferroelastic materials.[70]

The new terminology (MLSD and SLSD) is illustrated below in an analysis of the transformation mechanism considering the highly cooperative ($J_2 = 2.05$), moderately cooperative ($J_2 = 1.25$), and weakly cooperative cases ($J_2 = 0.5$).

Snapshots of the configuration of the system in the highly cooperative case are given in Fig. 5. In the first stage of the relaxation, two nuclei of molecules with the LS electronic configuration are formed at corners of the system, MLSDs

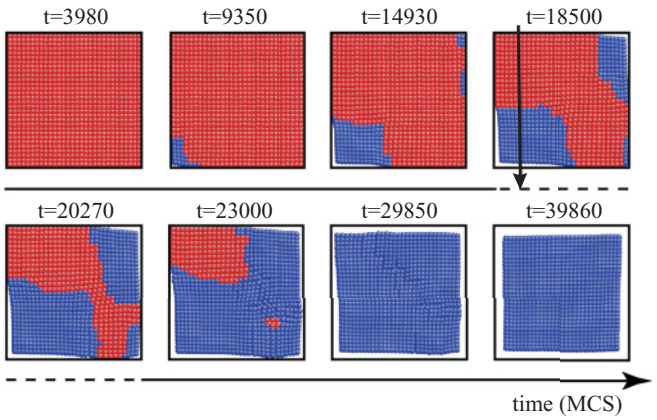

FIG. 5. (Color online) Instantaneous configuration of the system (spin and lattice) during thermal relaxation in the highly cooperative case [strong elastic coupling ($J_2 = 2.05$)]. LS and HS molecules are denoted as blue and red circles respectively. The vertical arrow at $t = 18500$ MCS indicates the position of the profiles depicted in Fig. 15. The outmost square gives the size of the system at $t = 0$.

subsequently grow until $t = 29\,850$ MCS. The spin state change is followed by a contraction of the structural lattice from the HS ($r^{norm} = 1$) to the LS ($r^{norm} \to 0$) lattice spacing values, leading to a progressive decrease of the overall volume, which persists till $t = 39\,860$ MCS, that is to say well after the HS-to-LS molecular state switching is complete. This is consistent with the delay between n_{HS} and r^{norm} relaxation curves discussed above.

Although the present elastic model contains both short-range and effective long-range interactions, nucleation phenomenon starts from the corners of the system, which is the signature of boundary conditions effects and the presence of elastic distortions.[53,54,71] The mechanisms of nuclei formation seem to be different for the elastic models by comparison with short-range Ising-like schemes. It has already been shown that in the case of a purely elastic model Hamiltonian on a system with periodic boundary conditions, clusters are suppressed and molecular state switching occurs uniformly in the lattice.[56] The situation may be different with the anharmonic elastic model, where LSDs are expected even with periodic boundary conditions. The propagation of the domain walls is driven by thermal fluctuations. In such cases, the average dimension R of the domains may follow a power law of the form $R \propto t^{\alpha}$. For such a highly cooperative case, SLSD superimposed almost with MLSD as can be seen at $t = 18\,500$ MCS for instance. Domain coalescence occurs around $t = 20\,000$–$23\,000$ MCS. It is important to stress that a structural reconstruction occurs in the late stage of the HS to LS relaxation; structural coherence is recovered at completeness of the transition. The cohesive potential $J_0 \times V_{elast}$ in the Hamiltonian is most probably the driving force for this late stage structural reconstruction.

The temporal evolution of the spin and lattice correlation functions, defined in Sec. II A, brings new insights on the mechanism of the relaxation process. The evolution of the fraction of HS-LS pairs, n_{HL}, is given in Fig. 6 for strong J_2 values. All curves exhibit a similar trend, characterized first by a rapid raise of the HS-LS pairs to a maximum, and then a slower decrease to zero at completeness of the HS to LS relaxation. The position of the maximum is displaced to shorter time and higher value when J_2 decreases. In this case of highly cooperative systems, the evolution of n_{HL} can be interpreted in the framework of the critical droplet classical

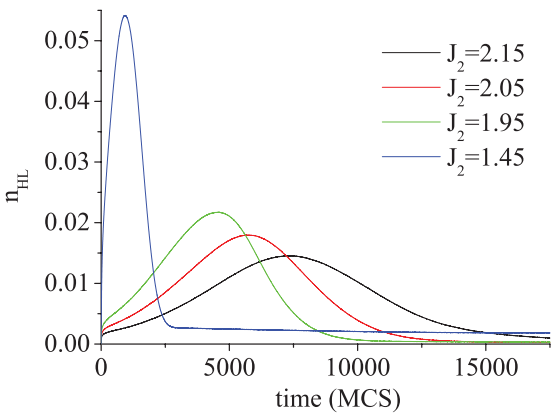

FIG. 6. (Color online) Temporal evolution of the fraction of HS-LS pairs n_{HL} for strong values of the J_2 parameter.

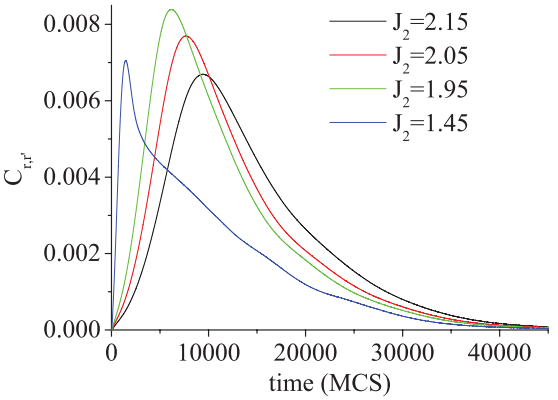

FIG. 7. (Color online) Temporal evolution of the lattice spatial correlation function $C_{r,r'}$ for strong values of the J_2 parameter.

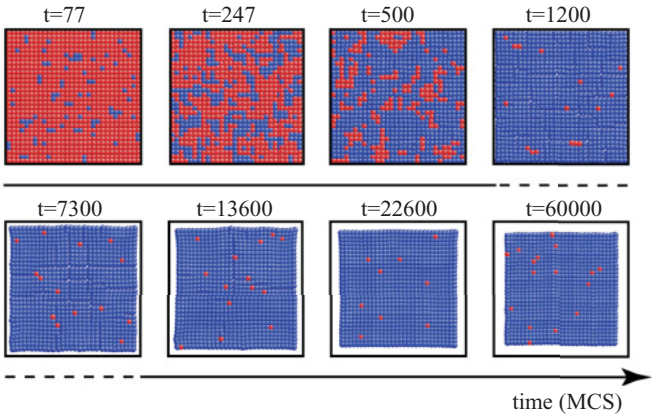

FIG. 8. (Color online) Evolution of the lattice and spin system configuration at different times during thermal relaxation in the case of a weakly cooperative system ($J_2 = 0.5$). LS and HS molecules are denoted as blue and red circles, respectively. The outmost square gives the size of the system at $t = 0$.

theory.[72] First, thermal fluctuations lead to the nucleation of the thermodynamically stable LS phase, leading to a rapid increase of HS-LS first neighbors. At this stage, "germ nuclei" are energetically unfavourable and do not reach the critical size above which domain growth occurs. Close to the maximum, critical nuclei are formed through favorable fluctuations,[73] LS domains develop. The maximum of HS-LS pairs fraction n_{HL} is reached when the total length of interface separating the HS and LS MLSD becomes maximal. Then, these growing domains coalesce, n_{HL} finally decreases. As J_2 increases in comparison with thermal fluctuations, the critical size for the germ nuclei is hard to attain, the maximum is displaced to a longer time. In parallel, the maximum value decreases, owing to the strong ferroelastic coupling, which favors HS-HS and LS-LS pair formation, leading to a higher MSLD size and lower length of the interface. These results are comparable to the numerical or analytical results provided by the standard Ising-like model[22,26] for the spin spatial correlation function.

As n_{HL} gives information on the distribution of HS and LS electronic states, and therefore on the MLSD, the inspection of the lattice spatial correlation function $C_{r,r'}$, given in Fig. 7 for strong values of the J_2 parameter, is complementary. As for the HS-LS pair fraction n_{HL}, the correlation function $C_{r,r'}$ exhibits a maximum, whose position depends on the cooperativity. A nonzero value of $C_{r,r'}$ indicates that elastic distortions occur within the system. These maxima are located at longer time with respect to n_{HL}, reflecting the delay of the lattice response with respect to the spin state change. The progressive formation of LS MSLD induces a built up of internal pressure in the system, due to the structural misfit of LS molecules within the HS structural matrix. Structural distortions set up, $C_{r,r'}$ therefore increases. After reaching a maximum, $C_{r,r'}$ decreases as the structural relaxations span the entire system. The long tail of the structural correlation function corresponds to the crystal lattice reconstruction in the late stage while the system is totally in the LS electronic configuration.

Instantaneous configurations of the system in the case of weak J_2 values are represented on Fig. 8 for different instants of the thermal relaxation. We have seen in Sec. III A that, for such a case, the spin and lattice variables are temporally decorrelated. Switching of HS molecules to the LS state occurs within the first 200 MCS, whereas the lattice has not reacted yet. Indeed, we may distinguish already formed LS clusters at $t = 247$ MCS. A close to homogeneous and uniform compression of the intersite distances, inducing a homogeneous decrease of the whole volume, only begins around $t = 2500$ MCS and is completed around $t = 45\,000$ MCS. No MLSD or SLSD can be distinguished along the relaxation.

The amplitude and position of the maximum of the HS-LS pairs fraction n_{HL} (see Fig. 9), follow a similar behavior to those already analyzed on Fig. 6, with nevertheless some important differences. First, the value of the HS-LS pairs fraction at the maximum is much higher, and the maximum position occurs at shorter time. In such a weakly cooperative case, as snapshots of the system do not evidence any MLSD, the transition mechanism is dominated by a homogeneous nucleation process of the thermodynamically stable LS phase, which leads to a rapid formation of numerous HS-LS pairs spread uniformly within the system. MLSD growth is hindered by thermal fluctuation, overcoming the weak ferroelastic interactions. As J_2 decreases, the fraction of HS-LS pairs at longer time increases, corresponding to the presence of HS residual species.

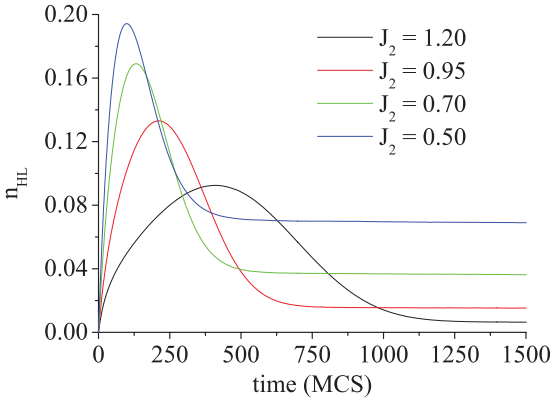

FIG. 9. (Color online) Temporal evolution of the fraction of HS-LS pairs n_{HL} for different weak values of the J_2 parameter.

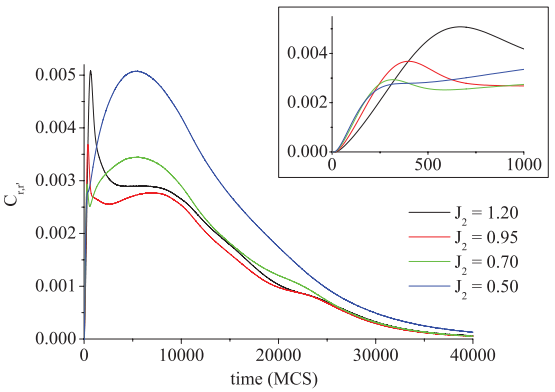

FIG. 10. (Color online) Temporal evolution of the lattice spatial correlation functions $C_{r,r'}$ for different weak values of the J_2 parameter. The insert corresponds to a zoom of $C_{r,r'}$ at short time ($0 < t < 1000$).

The behavior of the $C_{r,r'}$ lattice spatial correlation function (see Fig. 10) is more complicated with respect to the case of strong J_2 values. The maximum of $C_{r,r'}$ occurs at very short time ($t < 1000$ MCS) followed by a second maximum around $t = 7000$ MCS for $J_2 \leqslant 0.95$. The first maximum proceeds jointly with the nucleation process discussed for n_{HL}, while the second maximum and subsequent long tail in $C_{r,r'}$ corresponds more likely to late structural reconstruction.

C. Mapping of local lattice strain

It is evident from Fig. 5, that the development of SLSD is followed by structural distortions, notably at the domain boundaries. Figures 11–14 depict a quantitative mapping of the local strain as a function of time in the highly ($J_2 = 2.05$), weakly ($J_2 = 0.5$), and moderately cooperative ($J_2 = 1.25$) situations, respectively. High-strain values are associated to molecules for which the spatial distribution of the nearest neighbors differs severely from the ideal reference positions. For instance, a LS molecule surrounded by four neighbors at a distance of nearly r^0_{HS} exhibits a high positive strain value. For the highly cooperative case (see Fig. 11), by comparison with the configurations of the system depicted in Fig. 5, the development of high strain is associated to the nucleation and growth of MLSDs. The highest strain values are located at the MLSD boundaries, which correspond to molecules switching their electronic configuration from HS to LS while the lattice spacings in their immediate neighborhood is still close to r^0_{HS}. As these MLSD boundaries propagate in the system as a function of time during the HS to LS relaxation, a front of large structural strain propagates meanwhile. Deep in the growing MLSD, the structure is relaxing with spacing distances close to the equilibrium LS value, the local strain reduces in parallel. Interestingly, significant strain develops also in advance of the propagating MLSD boundary (for instance at $t = 18\,500$ MCS), as a precursor effect for the domain growth. The relaxation in this highly cooperative case occurs with the nucleation and growth of only two large MLSDs, which coalesce between $t = 20\,270$ and $23\,000$ MCS. The coalescence leaves high residual strain in the center of the system, which persists well after all the molecules are converted to the LS electronic state. The late stage of the relaxation corresponds to a release of this residual strain, which parallels a global size reduction of the deformable lattice to the equilibrium structural configuration of the purely LS phase. Obviously, the delay discussed above between the relaxation of the HS fraction and the normalized lattice spacing r^{norm} may be attributed to the release of the accumulated residual strain. It is noteworthy that the release of residual strain starts from the corners of the system, resulting most probably from the open boundary conditions used in our simulations. The accumulation of high strains at the domain walls characterized here has been recently observed by microscopy images using crossed polarizer, detecting birefringence of regions deformed by elastic strain and stress,[39] and has been interpreted as an acoustic wave that propagates in an elastic medium.

A very different situation occurs for the weakly cooperative case (see Fig. 12). Here, molecules are switching their spin state at almost spatial random in the system (see Fig. 8), no MLSD may be detected. For each LS site, a high strain develops purely locally. Contrary to the highly cooperative case, strain is limited to the LS molecule and does not propagate easily to the neighboring molecules. This is obviously due to the weak intermolecular interactions (weak J_2), a molecule switching its spin state does not perturb the structural configuration of its immediate neighborhood. At

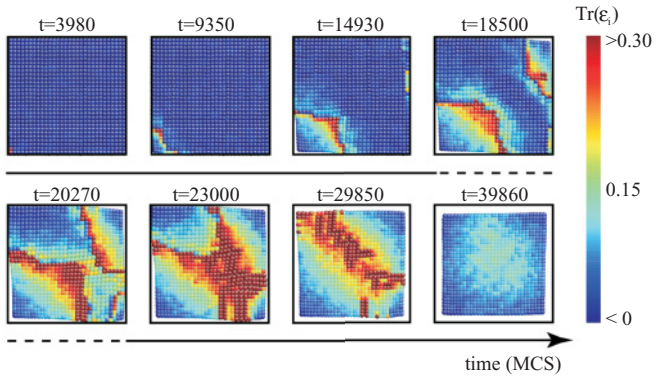

FIG. 11. (Color online) Spatial mapping of the strain value [Tr (ϵ_i)] during thermal relaxation in the highly cooperative case ($J_2 = 2.05$).

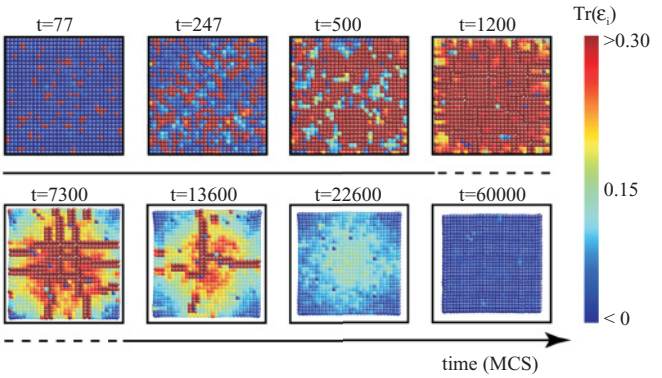

FIG. 12. (Color online) Spatial mapping of the strain value [Tr (ϵ_i)] during thermal relaxation in the weakly cooperative case ($J_2 = 0.5$).

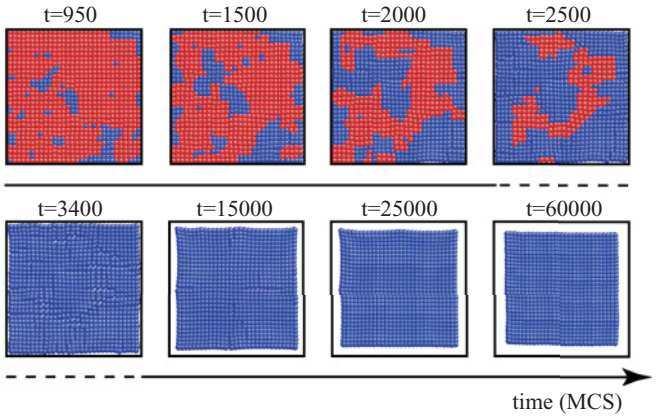

FIG. 13. (Color online) Evolution of the lattice and spin system configuration at different times during thermal relaxation in the case of a moderately cooperative system ($J_2 = 1.25$). LS and HS molecules are denoted as blue and red circles respectively. The outmost square gives the size of the system at $t = 0$.

$t = 1200$ MCS, all the molecules are in the LS electron configuration (see Fig. 8), while the entire system exhibits large strain values; this residual strain is relaxed later on, starting from the corners of the system.

It is interesting to compare the structural characteristics of the relaxation in a moderately cooperative case ($J_2 = 1.25$) with respect to the two situations discussed above. This moderately cooperative case exhibits an abrupt thermal spin transition, without any noticeable hysteresis (see Fig. 1). However, the development of MLSD is fundamentally different from the highly cooperative situation. In the latter case, only few domains nucleate at the boundary of the system and grow, while for $J_2 = 1.25$, several MLSD nucleate within the system and develop (see Fig. 13). Around $t = 3400$ MCS, the system is completely in the LS electronic configuration, but the corresponding lattice spacings are still much closer to the HS value. Starting from $t = 3400$ MCS, the size of the system progressively decreases until all the intersite distances are quite close to the equilibrium LS value. Large strain values are associated to the forming MLSDs, strain relaxation occurs after the HS to LS electronic configuration relaxation is completed around $t = 3400$ MCS. Slight strain increase is observed ahead of the propagating MLSD boundaries, as for the highly cooperative case.

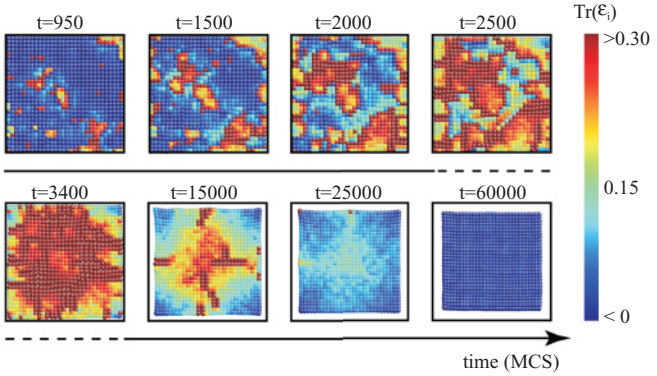

FIG. 14. (Color online) Spatial mapping of the strain value [Tr (ϵ_i)] during thermal relaxation in the moderately high cooperative case ($J_2 = 1.25$).

D. Structure of the domain wall

The structural distortions associated to domain walls in ferroelastic materials, such as wall thickness and strain distribution, are essential parameters that govern the walls energy and the microscopic domain pattern as well as the interactions of the domain walls with crystal defects. The spontaneous strain at domain walls may be estimated from the Landau free energies; the corresponding profile of the order parameter across the wall is found continuous of the form $\tanh(x/W)$ with W the wall thickness,[74–76] which is indeed observed experimentally for twin walls.[77] In the context of SCO materials, the structure of domain walls and their interaction with defects, such as dislocations and impurities, may have important implication on the dynamics of domain

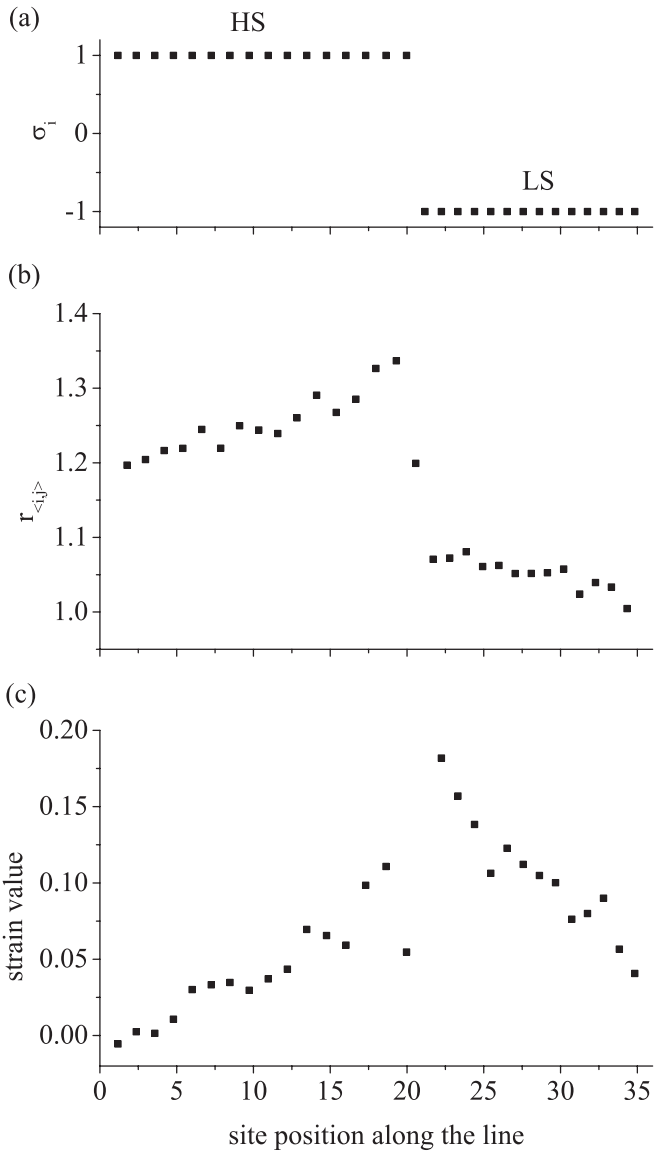

FIG. 15. Profile of the (a) spin variable σ_i, (b) intersite distance $r_{\langle i,j\rangle}$, and (c) strain value Tr (ϵ_i) along the vertical arrow depicted in Fig. 5 at $t = 18\,500$ MCS.

nucleation and growth. The impurity effect can be induced by replacement (dilution) of the Fe(II) SCO active molecules with isostructural Zn(II) or Co(II) analogues that do not present SCO. It has been shown by time- and temperature-dependent crystallographic analysis that the activation energy to domain growth is indeed perturbed with dilution.[31]

We have defined the above two concepts of domains, with respect to the two variables of our model: MLSD and SLSD. It is relevant to analyze under details the profiles of the spin and lattice variables in the neighborhood of the domain boundaries. For that purpose, we give in Fig. 15 the profiles of the spin variable σ_i, lattice variable $r_{\langle i,j\rangle}$, and strain value $\mathrm{Tr}\,(\epsilon_i)$ along the vertical arrow depicted in Fig. 5 for the highly cooperative case. The MLSD boundary is associated to an abrupt increase of the σ_i value from -1 inside the growing LS domain to $+1$ in the direction of the HS matrix [see Fig. 15(a)]. In parallel, the intersite distance almost abruptly increases from nearly 1.05 to 1.35 with only one intermediate value in the SLSD boundary; the transition region of the SLSD boundary is thus found quite sharp [see Fig. 15(b)]. Interestingly, the location of the MLSD and SLSD boundaries match perfectly with each other. Ahead of the SLSD boundary in the not yet converted HS region, the intersite distances are larger than the equilibrium $r^0_{\mathrm{HS}} = 1.2$ value and correspond to the build up of strain ahead of the propagating SLSD boundary. The decrease of intersite distances in the forming LS domain is compensated by this increase of the intersite distances in the HS phase. This is energetically allowed by the anharmonic shape of the intersite Lennard-Jones potential V_{elast}. The strain profile [see Fig. 15(c)] exhibits a large transition region, with a maximum at the boundary of the domain, a progressive decrease of strain from the boundary to almost 0.0 in the still unconverted HS phase, and a progressive decrease to a significant residual strain value in the forming LS domain.

IV. CONCLUSION

We have studied the high-spin to low-spin relaxation phenomenon in spin crossover molecular solids using out-of-equilibrium Monte Carlo simulations of a recently introduced anharmonic Ising-like Hamiltonian. The model is based on coupled electronic (spin state) and structural degrees of freedom of interacting spin crossover entities on a deformable lattice, accounting for the structural lattice distortions. The concept of like-spin domain emerges directly from this two variable scheme. A distinction between electronically defined (MLSD) and structurally defined (SLSD) domains is proposed.

By fine tuning, the elastic coupling J_2 of the model, SCO materials from high cooperativity to weak cooperativity can be described. In the former case, the sigmoidal relaxation kinetics of the high spin fraction n_{HS}, is retrieved, while the mean lattice spacing r^{norm} follows a similar, albeit delayed, trend. As the cooperativity progressively weakens (decreasing J_2), the lifetime of the metastable HS state decreases, the sigmoidal kinetics is maintained but the rate of relaxation increases. A further decrease of J_2 induces a loss of the sigmoidal character, while a temporal decoupling between the electronic and structural variables occurs. This decoupling has already been observed experimentally, and may found important applications to interpret time-resolved spectroscopic or diffraction experiments.

In the highly cooperative case, the spin transition proceeds through nucleation and growth of few domains of molecules with the LS electronic configuration, accompanied by lattice distortions. A front of high lattice strain is associated to the MLSD and propagates in parallel to the domain boundary during the HS to LS relaxation. Lattice strain is also observed ahead of the domain boundary. No MLSD nor SLSD are observed in the weakly cooperative case, while the development of lattice strain is essentially local and does not propagate within the system. In all cases, residual strain is progressively built up in the system during the relaxation, and released in the late stage of the relaxation through a structural phase rebuilding process driven by the cohesive potential $J_0 \times V_{\mathrm{elast}}$ in the Hamiltonian.

Our work provides the basis for interpreting the dynamics of phase transformations in spin transition materials and investigate the nucleation and growth of structural like-spin domain. It gives the first relation between mesoscopic and microscopic processes through the local strain mapping. A quantitative comparison between simulated diffraction pattern and experimental diffraction pattern may be very informative with that respect. This work is under progress and will be published in a forthcoming paper.

ACKNOWLEDGMENTS

This work was supported by the European Network of Excellence MAGMANet (FP6-515767-2), the Université Henri Poincaré, and the CNRS. The authors would like to thank K. Boukheddaden for helpful discussion. Part of the numerical calculations was performed at the computing center of the Institut Jean Barriol, Nancy, which is acknowledged.

*sebastien.pillet@crm2.uhp-nancy.fr

[1] L. Bogani and W. Wernsdorfer, Nat. Mater. **7**, 179 (2008).

[2] *Spin Crossover in Transition Metal Compounds*, edited by P. Gütlich and H. A. Goodwin, Top. Curr. Chem. 233–235 (Springer, New York, 2004).

[3] E. Meissner, K. Köppen, H. Spiering, and P. Gütlich, Chem. Phys. Lett. **95**, 163 (1983).

[4] V. Ksenofontov, A. B. Gaspar, and P. Gütlich, Top. Curr. Chem. **235**, 23 (2004).

[5] Y. Garcia, O. Kahn, J. P. Adler, A. Buzdin, Y. Meurdesoif, and M. Guillot, Phys. Lett. A **271**, 145 (2000).

[6] A. Bousseksou, F. Varret, M. Goiran, K. Boukheddaden, and J. P. Tuchagues, Top. Curr. Chem. **235**, 65 (2004).

[7] S. Bonhommeau, G. Molnar, A. Galet, A. Zwick, J. A. Real, J. J. McGarvey, and A. Bousseksou, Angew. Chem. Int. Ed. **44**, 4069 (2005).

[8] E. Freysz, S. Montant, S. Létard, and J.-F. Létard, Chem. Phys. Lett. **394**, 318 (2004).

[9] S. Decurtins, P. Gütlich, C. P. Köhler, and H. Spiering, Chem. Phys. Lett. **105**, 1 (1984).
[10] A. Hauser, Chem. Phys. Lett. **124**, 543 (1986).
[11] H. Spiering, T. Kohlhaas, H. Romstedt, A. Hauser, C. Bruns-Yilmaz, J. Kusz, and P. Gütlich, Coord. Chem. Rev. **190**, 629 (1999).
[12] H. Spiering, Top. Curr. Chem. **235**, 171 (2004).
[13] J. A. Real, A. B. Gaspar, V. Niel, and M. C. Munoz, Coord. Chem. Rev. **236**, 121 (2003).
[14] A. Hauser, Chem. Phys. Lett. **192**, 65 (1992).
[15] A. Hauser, Top. Curr. Chem. **234**, 155 (2004).
[16] O. Roubeau, J. G. Haasnoot, J. Linares, and F. Varret, Mol. Cryst. Liq. Cryst. **335**, 541 (1999).
[17] V. Mishra, R. Mukherjee, J. Linares, C. Baldé, C. Desplanches, J.-F. Létard, E. Collet, L. Toupet, M. Castro, and F. Varret, Inorg. Chem. **47**, 7577 (2008).
[18] A. Hauser, J. Jeftic, H. Romstedt, R. Hinek, and H. Spiering, Coord. Chem. Rev. **190**, 471 (1999).
[19] J. Wajnflasz and R. Pick, J. Phys. IV (France) **32**, C1 (1971).
[20] A. Bousseksou, J. Nasser, J. Linares, K. Boukheddaden, and F. Varret, J. Phys. I (France) **2**, 1381 (1992).
[21] J. Linares, H. Spiering, and F. Varret, Eur. Phys. B **10**, 271 (1999).
[22] I. Shteto, K. Boukheddaden, and F. Varret, Phys. Rev. E **60**, 5139 (1999).
[23] K. Boukheddaden, I. Shteto, B. Hôo, and F. Varret, Phys. Rev. B **62**, 14796 (2000).
[24] K. Boukheddaden, J. Linares, H. Spiering, and F. Varret, Eur. Phys. J. B **15**, 317 (2000).
[25] K. Boukheddaden, I. Shteto, B. Hôo, and F. Varret, Phys. Rev. B **62**, 14806 (2000).
[26] B. Hôo, K. Boukheddaden, and F. Varret, Eur. Phys. J. B **17**, 449 (2000).
[27] M. Sorai and S. Seki, J. Phys. Chem. Solids **35**, 555 (1974).
[28] S. Pillet, J. Hubsch, and C. Lecomte, Eur. Phys. J. B **38**, 541 (2004).
[29] S. Pillet, V. Legrand, M. Souhassou, and C. Lecomte, Phys. Rev. B **74**, 140101 (2006).
[30] K. Ichiyanagi, J. Hebert, L. Toupet, H. Cailleau, P. Guionneau, J.-F. Létard, and E. Collet, Phys. Rev. B **73**, 060408 (2006).
[31] G. Lebedev, S. Pillet, C. Baldé, P. Guionneau, C. Desplanches, and J.-F. Létard, IOP Conf. Series: Mater. Sci. Eng. **5**, 012025 (2009).
[32] K. Nakano, S. Kawata, K. Yoneda, A. Fuyuhiro, T. Yagi, S. Nasu, S. Moritomo, and S. Kaizaki, Chem. Commun. 2892 (2004).
[33] M. Buron-LeCointe, N. OuldMoussa, E. Trzop, A. Moreac, G. Molnar, L. Toupet, A. Bousseksou, J. F. Letard, and G. S. Matouzenko, Phys. Rev. B **82**, 214106 (2010).
[34] N. Brefuel, H. Watanabe, L. Toupet, J. Come, N. Matsumoto, E. Collet, K. Tanaka, and J. P. Tuchagues, Angew. Chem. Int. Ed. **48**, 9304 (2009).
[35] S. Pillet, C. Lecomte, C. F. Sheu, Y. C. Lin, I. J. Hsu, and Y. Wang, J. Phys. Conf.: Series. **21**, 221 (2005).
[36] A. Goujon, F. Varret, K. Boukheddaden, C. Chong, J. Jeftic, Y. Garcia, A. D. Naik, J. C. Ameline, and E. Collet, Inorg. Chim. Acta **361**, 4055 (2008).
[37] C. Chong, A. Slimani, F. Varret, K. Boukheddaden, E. Collet, J. C. Ameline, R. Bronisz, and A. Hauser, Chem. Phys. Lett. **504**, 29 (2011).
[38] A. Slimani, F. Varret, K. Boukheddaden, C. Chong, H. Mishra, J. Haasnoot, and S. Pillet, Phys. Rev. B **84**, 094442 (2011).
[39] S. Bedoui, G. Molnar, S. Bonnet, C. Quintero, H. J. Shepherd, W. Nicolazzi, L. Salmon, and A. Bousseksou, Chem. Phys. Lett. **499**, 94 (2010).
[40] H. Watanabe, H. Hirori, G. Molńar, A. Bousseksou, and K. Tanaka, Phys. Rev. B **79**, 180405 (2009).
[41] H. Watanabe, N. Bréfuel, S. Mouri, J.-P. Tuchagues, E. Collet, and K. Tanaka, Europhys. Lett. **96**, 17004 (2011).
[42] M. Lorenc, J. Hébert, N. Moisan, E. Trzop, M. Servol, M. Buron-Le Cointe, H. Cailleau, M. L. Boillot, E. Pontecorvo, M. Wulff, S. Koshihara, and E. Collet, Phys. Rev. Lett. **103**, 028301 (2009).
[43] S. Nozawa, T. Sato, M. Chollet, K. Ichiyanagi, A. Tomita, H. Fujii, S. Adachi, and S. Koshihara, J. Am. Chem. Soc. **132**, 61 (2010).
[44] A. Cannizzo, C. J. Milne, C. Consani, W. Gawelda, C. Bressler, F. van Mourik, and M. Chergui, Coord. Chem. Rev. **254**, 2677 (2010).
[45] K. Boukheddaden, S. Miyashita, and M. Nishino, Phys. Rev. B **75**, 094112 (2007).
[46] Y. Konishi, H. Tokoro, M. Nishino, and S. Miyashita, Phys. Rev. Lett. **100**, 067206 (2008).
[47] W. Nicolazzi, S. Pillet, and C. Lecomte, Phys. Rev. B **78**, 174401 (2008).
[48] K. Boukheddaden, M. Nishino, and S. Miyashita, Phys. Rev. Lett. **100**, 177206 (2008).
[49] C. Enachescu, L. Stoleriu, A. Stancu, and A. Hauser, Phys. Rev. Lett **102**, 257204 (2009).
[50] J. A. Nasser, Eur. Phys. J. B **21**, 3 (2001).
[51] M. Nishino, K. Boukheddaden, Y. Konishi, and S. Miyashita, Phys. Rev. Lett. **98**, 247203 (2007).
[52] M. Nishino, K. Boukheddaden, and S. Miyashita, Phys. Rev. B **79**, 012409 (2009).
[53] M. Nishino, C. Enachescu, S. Miyashita, K. Boukheddaden, and F. Varret, Phys. Rev. B **82**, 020409 (2010).
[54] C. Enachescu, M. Nishino, S. Miyashita, L. Stoleriu, A. Stancu, and A. Hauser, Europhys. Lett. **91**, 27003 (2010).
[55] W. Nicolazzi, S. Pillet, and C. Lecomte, Phys. Rev. B **80**, 132102 (2009).
[56] S. Miyashita, Y. Konishi, M. Nishino, H. Tokoro, and P. A. Rikvold, Phys. Rev. B **77**, 014105 (2008).
[57] E. Buhks, M. Bixon, and J. Jortner, J. Am. Chem. Soc. **109**, 2918 (1980).
[58] M. Nishino, K. Boukheddaden, S. Miyashita, and F. Varret, Phys. Rev. B **68**, 224402 (2003).
[59] N. Klinduhov, D. Chernyshov, and K. Boukheddaden, Phys. Rev. B **81**, 094408 (2010).
[60] M. G. Buendìa, P. A. Rikvold, K. Park, and M. A. Novotny, J. Chem. Phys. **121**, 4193 (2004).
[61] H. C. Kang and W. H. Weinberg, J. Chem. Phys. **90**, 2824 (1989).
[62] P. M. Gullett, M. F. Horstemeyer, M. I. Baskes, and H. Fang, Modelling Simul. Mater. Sci. Eng. **16**, 015001 (2008).
[63] F. Shimizu, S. Ogata, and J. Li, Materials Transactions **48**, 2923 (2007).
[64] V. Legrand, S. Pillet, C. Carbonera, M. Souhassou, J.-F. Létard, P. Guionneau, and C. Lecomte, Eur. J. Inorg. Chem. **2007** 5693 (2007).
[65] K. Boukheddaden, E. D. Loutete-Dangui, E. Codjovi, M. Castro, J. A. Rodriguez-Velemazan, S. Ohkoshi, H. Tokoro, M. Koubaa, Y. Abid, and F. Varret, J. Appl. Phys. **109**, 013520 (2011).
[66] M. Nishino, S. Miyashita, and K. Boukheddaden, J. Chem. Phys. **118**, 4594 (2003).

[67] A. Muraoka, K. Boukheddaden, J. Linares, and F. Varret, Phys. Rev. B **84**, 054119 (2011).
[68] L. Stoleriu, P. Chakraborty, A. Hauser, A. Stancu, and C. Enachescu, Phys. Rev. B **84**, 134102 (2011).
[69] F. Cooper, B. Freedman, and D. Preston, Nucl. Phys. B **210**, 210 (1982).
[70] J. Chrosch and E. K. H. Salje, J. Appl. Phys. **85**, 722 (1999).
[71] S. Miyashita, M. Nishino, Y. Konishi, H. Tokoro, K. Boukheddaden, F. Varret, and P. A. Rikvold, J. Phys.: Conf. Series. **148**, 012027 (2009).
[72] J. S. Langer, Ann. Phys. (NY) **41**, 108 (1967).
[73] J. Linares, J. Nasser, K. Boukheddaden, A. Bousseksou, and F. Varret, J. Magn. Magn. Mat. **140**, 1507 (1995).
[74] E. K. H. Salje, *Phase Transitions in Ferroelastic and Co-elastic Crystals* (Cambridge University Press, Cambridge, 1993).
[75] J. Novak and E. K. H. Salje, Eur. Phys. J. B **4**, 279 (1998).
[76] W. T. Lee and E. K. H. Salje, J. Appl. Phys. **93**, 9890 (2003).
[77] D. Shilo, G. Ravichandran, and K. Bhattacharya, Nat. Mater. **3**, 453 (2004).